scientific reports

Check for updates

OPEN

Reactions of a high explosive under low intensity impact with adjustable amplitude and duration

Wujiang Ying[1], Zhuoheng Li[2], Pan Liu[1], Feichao Miao[3], Lin Zhou[1] & Xiangrong Zhang[1]✉

Laboratory testing with adjustable loading amplitudes and durations remains the primary method for assessment of the safety of explosives under either launch or penetration environment. In this study, a novel impact testing laboratory equipment with loading amplitudes ranging from 0.1 to 1.0 GPa and pulse durations ranging from 1 to 8 ms is established. It was used to investigate the safety of a 2,4-dinitroanisole (DNAN)-based melt-cast explosive subjected to impact loading in either launch or penetration scenarios. The explosive's response to the impact loading depends not only on the loading characteristics (peak pressure and maximum rate of pressure rise) but also on the confinements of the explosives. The ignition events of the explosives exhibited some randomness. A logistic regression analysis method was utilized to analyze such ignition events. This method can predict the ignition events of the DNAN-based melt-cast explosive with a high accuracy, which demonstrates the effectiveness of the method. The effect of the confinements of the explosives on the accuracy of this method was also investigated.

Keywords Impact testing, Explosives, Non-shock initiation, Logistic regression, Ignition discrimination, Cross-validation

An explosive charge, bare or in a projectile, is frequently subjected to all types of mechanical stimuli[1], and may be ignited if some criterion is satisfied. Mechanical stimuli can be approximately divided into two categories: shock and non-shock. The shock mechanical stimulus is characterized by a high amplitude (pressure on the order of several GPa or above) with a short pulse duration (on the order of several microseconds). The ignition of the explosive charge by a shock wave followed by growth to detonation is commonly termed as shock-to-detonation transition (SDT)[2]. In contrast, the non-shock mechanical stimulus is characterized by a low amplitude (pressure roughly on the order of 0.1–1 GPa) with a long pulse duration (on the order of several milliseconds)[3,4]. Compared to SDT, the ignition of the explosive charge by a non-shock mechanical stimulus can be termed as XDT (X stands for unknown)[5] or delayed detonation[6,7].

When a projectile charged with explosives penetrates a concrete target (not steel target) or is launched in an artillery, the corresponding explosive charge usually suffers from the mechanical stimulus, which is characterized by a low amplitude with a long pulse duration, as described above[8]. Therefore, it needs to be evaluated whether there is ignition of such a projectile in the penetration or launch process. Field testing of possible ignition events (XDTs) is the most direct approach for evaluation. However, as the ignition probability of such XDTs is low, field testing is not a realistic approach although it must remain the final criterion[9].

In this regard, laboratory testing is generally used to evaluate the penetration stability[4] or launch safety[10,11] of the projectile. Numerous laboratory equipments were designed and manufactured to analyze XDTs of projectiles[3,4,11–15]. Depending on whether the original energy source of the impact force loaded on an explosive sample is related to a drop hammer, these laboratory equipments can be broadly divided into two types: drop hammer and non-drop hammer. For the non-drop hammer-type equipment, gunpowder[13–16] or compressed air[4,11] is used as an original energy source. The load amplitude and pulse width applied to the explosive sample cannot be easily controlled. In contrast, for the drop hammer-type equipment[3,17], the drop hammer is the original energy source, and thus the whole equipment is vertically assembled. Furthermore, if the drop hammer is combined with compressed air, the load amplitude and pulse width can be relatively easily controlled.

2,4-dinitroanisole (DNAN)-based melt-cast explosives are widely used and are gradually replacing the traditional 2,4,6-trinitrotoluene (TNT)-based melt-cast explosives. DNAN-based melt-cast explosives exhibited

[1]State Key Laboratory of Explosion Science and Safety Protection, Beijing Institute of Technology, Beijing 100081, China. [2]CSSC System Engineering Research Institute, Beijing 100094, China. [3]State Key Laboratory of Explosion Science and Safety Protection, Anhui University of Science and Technology, Huainan 232001, China. ✉email: zhangxr@bit.edu.cn

characteristics of equivalent or improved extremely insensitive detonative substances compared to TNT-based melt-cast explosives, while maintaining the performance requirements of explosives[18,19]. Under the shock mechanical stimulus, the sensitivity of DNAN-based melt-cast explosives has been investigated[20,21]. However, under the non-shock mechanical stimulus characterized by a low amplitude and long pulse duration, the sensitivity of DNAN-based melt-cast explosives is yet to be thoroughly investigated.

This study focuses on the non-shock mechanical sensitivity of a DNAN-based melt-cast explosive (30 wt% HMX (cyclotetramethylene-tetranitramine), 40 wt% NTO (3-Nitro-1,2,4-triazol-5-one), 8 wt% Al (Aluminum), and 2 wt% MNA (N-methyl-p-nitroaniline) and other additives) tested by a unique laboratory equipment. Firstly, this equipment characterized by adjustable amplitudes and pulse durations was used to approximately mimic the load characteristics for the penetration or launch environment of an explosive charge in a projectile, as presented in detail in Section "Experiments". Secondly, logistic regression, a widely used statistical method for modeling of the probability a binary outcome based on one or more independent variables[22], was employed to analyze the ignition discrimination of the DNAN-based melt-cast explosive with the laboratory equipment. The effect of sample confinements on the ignition discrimination was further investigated.

Experiments

Experimental setup

As shown in Fig. 1, the impact testing laboratory equipment mainly consists of three modules: hammer loading module, pulse shaping module, and sample testing module. These three modules are assembled in order from top to bottom. The total weight of the whole equipment is approximately 800 kg. The equipment can provide an impact force with a load amplitude of 0.1–1.0 GPa and pulse width of 1–8 ms. Additionally, to avoid possible damage resulting from the reactions of explosive samples, blast resistance structures are generally installed[23–25]. In this study, the whole equipment was surrounded by simple steel walls (not shown in Fig. 1).

As shown in Fig. 2, the hammer loading module mainly consists of a drop hammer, compressed air chamber, and fixture. The drop hammer weights approximately 46 kg with a diameter of 200 mm and height of 333 mm. The compressed air chamber on the top of the drop hammer is connected to an outside high-pressure gas storage bottle. The output pressure of the compressed air chamber is in the range of 0–2 MPa with a precision of 0.01 MPa. The fixture is used to fix the drop hammer and control its release.

Pulse shaping module

As both drop hammer mass and height are fixed, the dynamic adjustment of either the load amplitude or pulse width should resort to other approaches. Although the load amplitude (peak pressure loaded on the samples) can be adjusted on the basis of the magnitude of the release pressure in the compressed air chamber, the pulse width can only be adjusted in a limited degree. To obtain a pulse width in a wider range, a pulse shaper was used in this study.

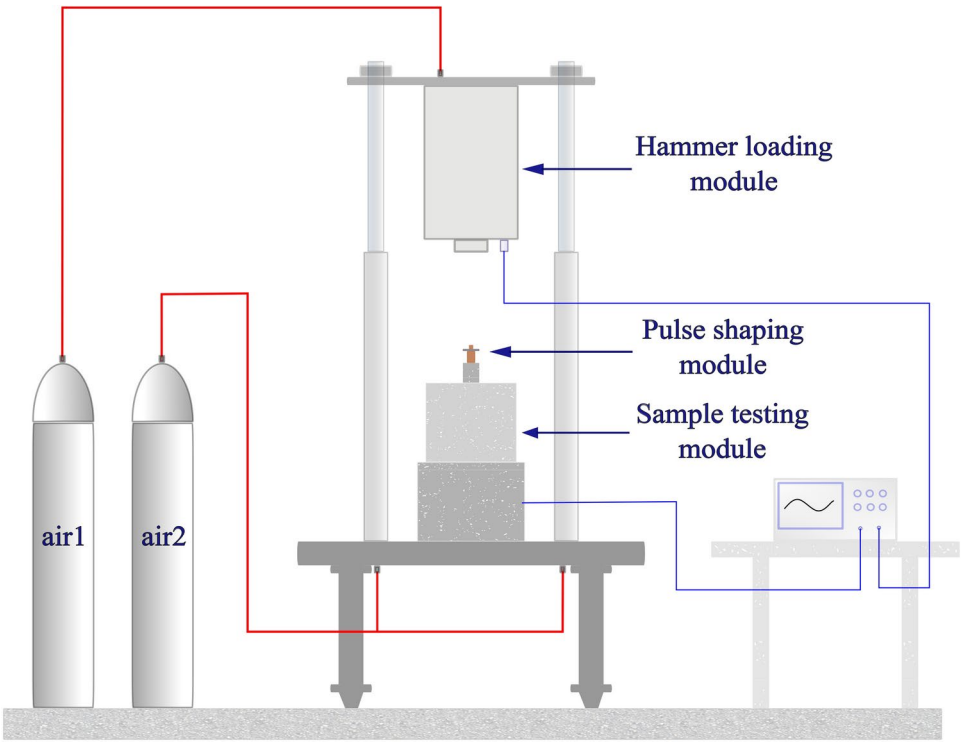

Fig. 1. Impact testing laboratory equipment.

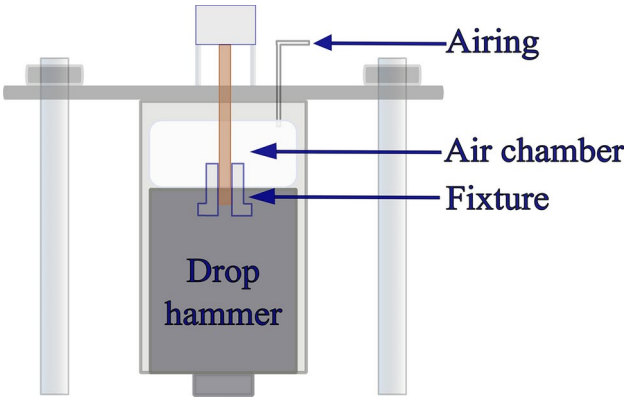

Fig. 2. Hammer loading module.

Fig. 3. Photograph of the pulse shaper.

No.	Top copper		Bottom copper		
	Diameter (mm)	Height (mm)	Inner diameter (mm)	Outer diameter (mm)	Height (mm)
1	–	–	–	14	18
2	–	–	–	18	22
3	–	–	–	22	22
4	–	–	–	22	30
5	10	10	–	18	22
6	10	10	–	22	30
7	10	10	7	22	22
8	10	10	7	22	30

Table 1. Copper cylinders with different sizes.

As shown in Fig. 3, the pulse shaper was composed of copper with an excellent ductility, though it can be also fabricated by different materials.

Depending on the pulse width requirements, the pulse shaper consists of one or two copper cylinders. When two copper cylinders are used, they are separated by a cylindrical thin sheet of silico-manganese steel. Generally, small and big copper cylinders are located on the top and bottom of the thin sheet, respectively. The copper cylinders can be solid or hollow with different sizes listed in Table 1.

Sample testing module

When the hammer drops, it acts on the pulse shaper, then on the upper plunger (if there is no pulse shaper, the hammer directly acts on the upper plunger), and finally on the explosive sample. An extrusion of explosive may occur between the plungers and rigid confinement cylinder resulting in an accident ignition of the explosive[26].

To avoid such occurrence of extrusion of explosive, a polyethylene (PE) slice is generally placed on each of the upper and lower surfaces of the explosive column, as shown in Fig. 4. Moreover, surfaces of the explosive sample were coated with a layer of silicone grease so that there is no gap or air around the explosive sample.

A pressure transducer was installed at the bottom of the lower plunger. Generally, even if the explosive sample does not undergo any reaction during the impact process, the pressure–time history is not the same at different coaxial locations because of wall friction effect. However, if the explosive sample reacts, these pressure–time curves should suddenly rise nearly at the same time.

If there is no soft confinement between the rigid confinement and sides of the explosive sample, a one-dimensional strain process can be assumed in the explosive sample upon impact, as shown in Fig. 4a. If there is a soft confinement inserted between the rigid confinement and sides of the explosive sample, the deformation process in the explosive sample is three-dimensional, as shown in Fig. 4b. In this study, a soft confinement (linear elastic material) was used, and the size of the soft confinement could be tailored (Section "Load characteristics subjected to the explosive samples").

The explosive sample used in this study has a diameter of 15 mm and height of 14 mm. As the size of the explosive sample is small, during the rapid solidification process of the molten suspension of the DNAN-based melt-cast explosive, there is no sufficient time for the air bubbles inside the molten suspension to escape outside, and the resulting densities of the explosive samples quite largely disperse.

To obtain explosive samples with a consistent density, the cooling and solidification rate of the molten suspension in a mold should be reduced and the mold should be vacuumed. In addition, sufficient explosive samples should be solidified at one time. To meet the above requirements, a group mold device was established, as shown in Fig. 5.

The device was connected with a constant-temperature water bath and vacuum pump. When the molten suspension of the DNAN-based melt-cast explosive prepared in advance was poured into the molds, a sealing plate was placed over the molds, and then vacuumed for 15 min. Based on the solidification process of the explosive suspension, the temperature in the water bath gradually decreased to room temperature according to a set procedure.

The explosive samples ground by a sandpaper are shown in Fig. 6. The densities of these samples were measured. The density deviation between these samples did not exceed 0.5%. The relative densities of these samples were larger than 97.5%, which demonstrates that the quality of the explosive samples was well controlled.

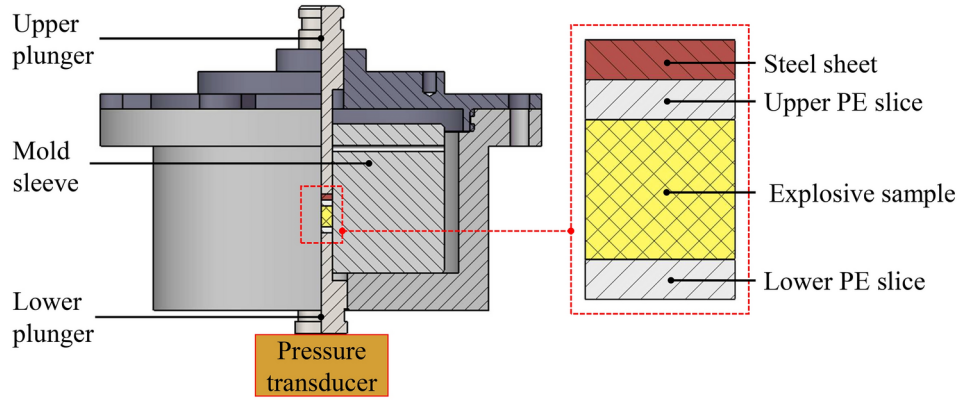

(a) Rigid confinement

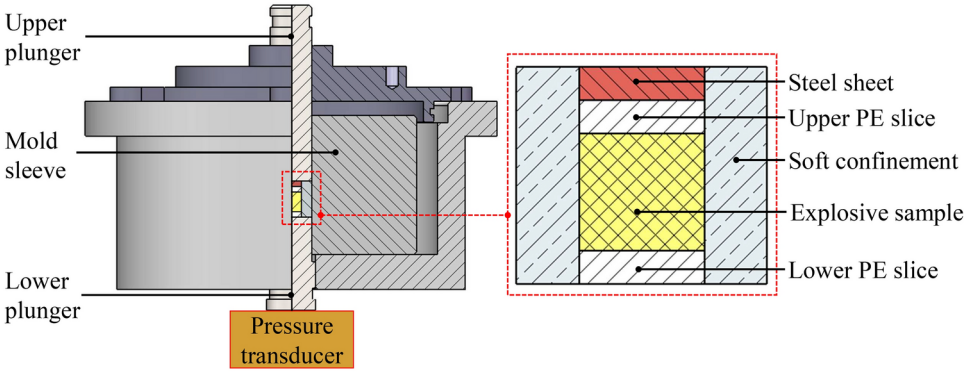

(b) Soft confinement

Fig. 4. Schematic diagram of the sample testing module.

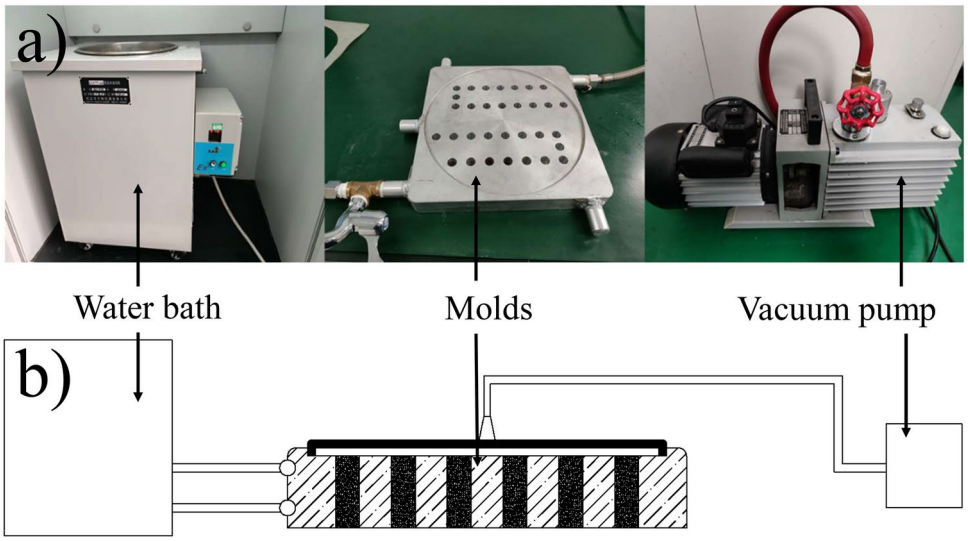

Fig. 5. Group mold device (**a**) Photograph of the group mold and (**b**) Schematic diagram of the group mold.

Fig. 6. Photograph of explosive samples.

Experimental procedures

Before the first test and every time when an impact test is completed, the status of the whole equipment should be inspected thoroughly to ensure that all parts of the equipment are normal. If any parts were damaged during the last impact test, they should be replaced with new. After the inspection, the procedures for the next impact test has the following main steps.

1. The explosive sample coated with a layer of silicone grease is placed inside the cylinder of the soft confinement (Fig. 4b). The inside of the cylinder of the rigid confinement, lower plunger, lower PE slice, explosive sample, upper PE slice, steel sheet, and upper plunger are installed sequentially.
2. The pulse shaper is placed on the top of the upper plunger. Regardless whether the pulse shaper consists of one or two copper cylinders, related parts were installed coaxially with the plungers. If a pulse shaper is not used in the impact test, this step can be omitted.
3. The compressed air chamber was inflated to given pressure. When the drop hammer was released by a switch, it was accelerated to fall vertically due to the pressure in the compressed air chamber. Both acceleration and pressure transducers were triggered, and the acceleration–time and pressure–time histories were recorded during the whole impact process.

Results and discussion

Input pressure–time curves

For convenience, we did not measure the input pressure on the supper surface of the explosive sample. Rather, we measured the pressure–time history at the bottom of the lower plunger. When the explosive sample was impacted with different amplitudes and pulse widths, these pressure–time curves can be used as a relative measure for the input pressure[3].

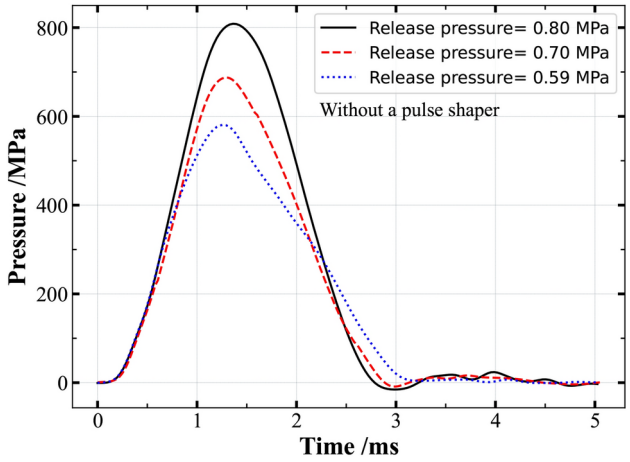

Fig. 7. Effect of the release pressure on the pressure–time history.

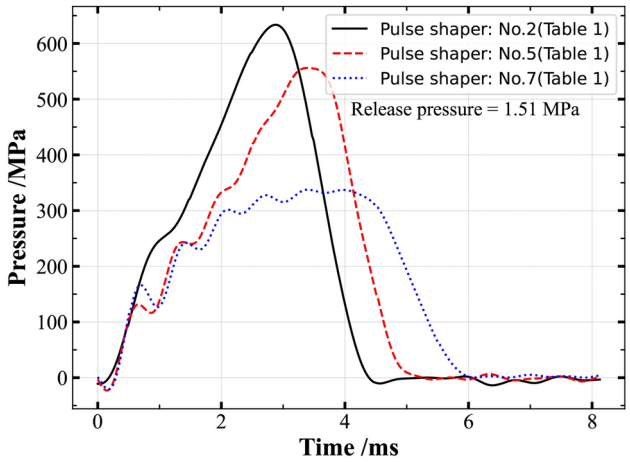

Fig. 8. Effect of the pulse shaper on the pressure–time history.

Figures 7 and 8 show the effects of release pressure (in the compressed air chamber) and pulse shaper on the pressure–time curves below the lower plunger, respectively.

As shown in Fig. 7, a typical pressure–time curve appears as half of a sine wave. The amplitudes of the three pressure–time curves increase with the release pressure in the compressed air chamber, while the pulse widths (approximately 3 ms) seem to be unaffected by the release pressure. In contrast, both amplitude and pulse width of the pressure–time curve can be adjusted with different pulse shapers, as shown in Fig. 8.

Sample response under given impact condition

Output pressure–time curves

If the explosive samples did not react upon impact, the pressure–time curves appeared as half sine waves (Figs. 7 and 8). If the explosive samples reacted, these curves deviated from the shape of half of a sine wave and suddenly raised before or after the peak was reached, as shown in Figs. 9a and b, respectively.

Videos of sample response upon impact

The experimental setup and process were videotaped. If the explosive sample did not react upon impact, no smoke or flame could be observed except that the impact sound of the drop hammer could be heard, as shown in Fig. 10a. If the explosive sample reacted upon impact, besides a strong sound, smoke (slight reaction) or flame (violent reaction) could be observed, as shown in Fig. 10b and c, respectively.

Recycled photographs of test samples

Figure 11 shows the photographs of the steel sheet, upper PE, lower PE, explosive sample, and soft confinement before (Fig. 11a) and after (Fig. 11b–d) the impact test.

If the explosive sample did not react upon impact, the soft confinement recovered well, while the sizes of the upper PE, explosive sample, and lower PE changed slightly. Their heights decreased within 5%, as shown in Fig. 11b. If the explosive sample reacted upon impact, both upper PE and lower PE were deformed largely (not

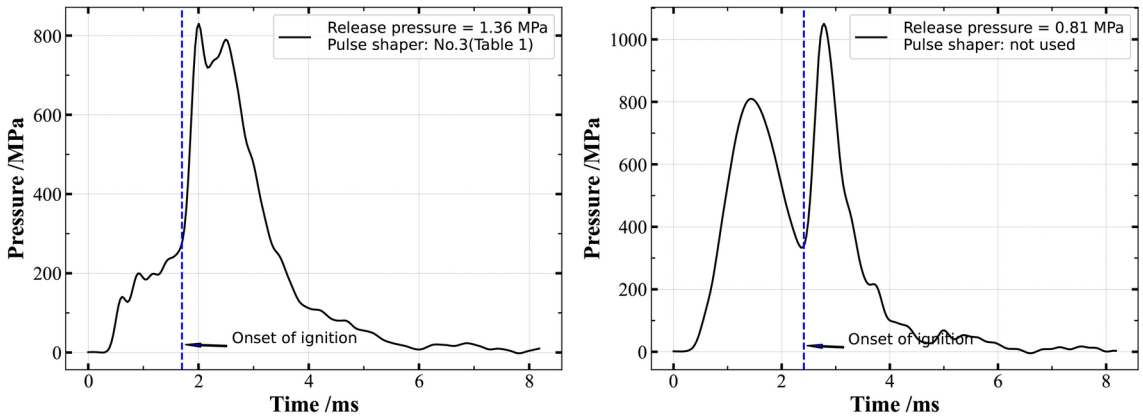

(a) Before the peak **(b)** After the peak

Fig. 9. Typical pressure–time history for the reacted explosive sample impact.

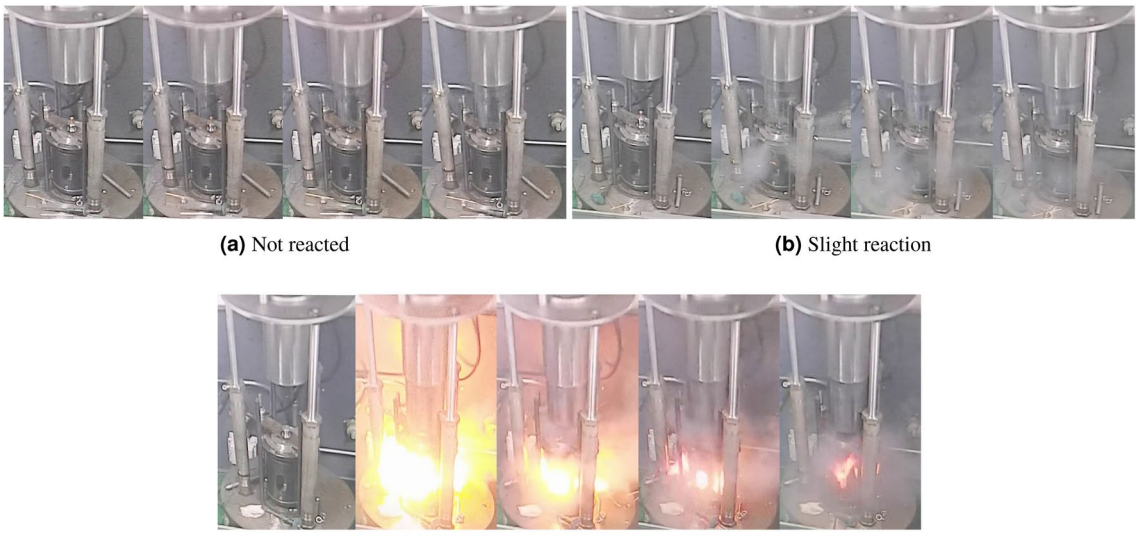

(a) Not reacted **(b)** Slight reaction

(c) Violent reaction

Fig. 10. Videos of sample response upon impact.

shown). Moreover, in an impact test with a slight reaction, only a small amount of black soot can be observed, as shown in Fig. 11c. In contrast, in an impact test with a violent reaction, no residues of the explosive sample can be observed, as shown in Fig. 11d.

Ignition discrimination analysis

Based on the videos and photographs in Figs. 10 and 11, the response of explosive samples upon impact can be broadly classified into two types: ignition (including both slight reaction and violent reaction, Fig. 10b and c) and absence of ignition (absence of reaction, Fig. 10a). The occurrence of ignition for the explosive sample upon impact is determined by many random factors, such as the microstructural morphology of the explosive sample[27]. Therefore, a probabilistic model, not a deterministic model, should be used to describe such ignition events. In this study, a logistic regression model was used to classify the ignition and non-ignition events for the explosive samples upon impact.

Logistic regression modeling

Logistic regression is a widely used statistical method for modeling of the probability of a binary outcome based on one or more independent variables[22]. Unlike linear regression, which predicts continuous outcomes, logistic regression predicts the probability of given input belonging to a particular class. This makes it particularly useful in medical research[28,29], finance[30,31], social sciences[32], and risk assessment and disaster management[33,34], where the outcomes are often binary (e.g., success/failure, yes/no, or presence/absence).

(a) Photographs of the steel sheet, upper PE, lower PE, explosive sample, and soft confinement before the impact test.

(b) No reaction, photographs of the steel sheet, upper PE, lower PE, explosive sample, and soft confinement after the impact test.

(c) Slight reaction **(d)** Violent reaction

Fig. 11. Photographs of test samples before and after the impact test.

The logistic regression model estimates the probability $P(Y = 1|\mathrm{X})$ as a function of the independent variables $\mathrm{X} = (X_1, X_2, \ldots, X_p)$. The relationship between the independent variables and probability is modeled using the logistic function, which ensures that the predicted probabilities are between 0 and 1. The logistic function is defined as[34,35]

$$P(Y = 1|\mathrm{X}) = \frac{1}{1 + e^{-(\beta_0 + \beta_1 X_1 + \beta_2 X_2 + \cdots + \beta_p X_p)}}, \tag{1}$$

where $P(Y = 1|\mathrm{X})$ is the probability that the outcome Y is 1 given the variables X, β_0 is the intercept term, and $\beta_1, \beta_2, \ldots, \beta_p$ are the coefficients associated with the independent variables $X_1, X_2, \ldots, X_p$.

In logistic regression, $P(Y = 1|\mathrm{X})$ is often converted into a binary outcome (0 or 1) using a probability cutoff value. The predicted binary variable is expressed by

$$\hat{Y} = \begin{cases} 1 & \text{if } P(Y = 1|\mathrm{X}) \geq \text{cutoff value} \\ 0 & \text{otherwise,} \end{cases} \tag{2}$$

where $\hat{Y}$ represents the predicted binary variable with 1 indicating the occurrence of ignition (GO) and 0 indicating absence of ignition (NO-GO). Generally, the cutoff value is set as 0.5 because of statistical benefits[34]. The choice of the optimal probability cutoff between ignition and non-ignition conditions is discussed in Section "Load characteristics subjected to the explosive samples". This choice is facilitated through a graph of sensitivity and specificity against each possible cutoff[35]. The sensitivity (true positive rate, TPR) is defined as the proportion of correctly predicted positive instances, where TPR is expressed as TP/(TP+FN), where TP and FN denote true positives (correctly predicted GO) and false negatives (incorrectly predicted NO-GO), respectively. Similarly, the specificity (true negative rate, TNR) is defined as the proportion of correctly predicted negative instances, where TNR is expressed as TN/(TN+FP), where TN and FP denote true negatives (correctly predicted NO-GO) and false positives (incorrectly predicted GO), respectively. This approach ensures that the cutoff choice, meant to predict GO and NO-GO from estimated probabilities, is quantitatively determined rather than subjectively chosen a priori[33,36].

The classification performance of the logistic regression model needs to be evaluated. As the experimental datasets (Tables 3 and 4) exhibited a significant imbalance with the number of NO-GO and GO/PPI, the stratified K-fold cross-validation (SK-CV) method was used to evaluate this model. Generally, the SK-CV method can ensure that each fold of the dataset contains approximately the same percentage of samples of each class as the

complete experimental dataset, making the training and validation process fair and more reliable[37]. This method splits the dataset into *K* folds. In each of the *K* iterations, one fold is used for testing while the remaining folds are used for training. In most cases, the value of *K* is set to 5 or 10[37]. In this study, we used stratified five-fold CV considering the size of the experimental dataset.

In evaluation of the classification performance of a model, accuracy, receiver operating characteristic (ROC) curve, and area under ROC curve (AUC) are widely used metrics[33,38,39]. The metrics were calculated from the confusion matrix[39]. The confusion matrix (Table 2) provides a comprehensive summary of the model's predictions compared to the actual outcomes. The accuracy defined as ((TN + TP)/N) represents the percentage of correctly classified test dataset, where N is the total number of datasets for validation (N = TP + FN + FP + TN).

The ROC curve is a graphical representation of the model's binary classification performance[37], with TPR on the y-axis against FPR on the x-axis over all possible cutoffs, where FPR is expressed as FP/(TN+FP). AUC serves as a global accuracy statistic for the model, independent of a single probability cutoff[36]. The AUC ranges from 0.5 (equivalent to random assignment, represented by the diagonal line) to 1.0 (perfect discrimination), providing a more comprehensive description of classification accuracy, particularly in imbalanced datasets[39].

The above three metrics (accuracy, ROC, and AUC) used to evaluate the classification performance of the logistic regression model for the explosive samples upon impact are presented in detail in Section "Load characteristics subjected to the explosive samples".

Load characteristics subjected to the explosive samples

As indicated in Eq. (1), the ignition probability for an explosive sample upon impact can be affected by many factors (independent variable X in Eq. (1)). However, for certain explosive sample with a fixed experimental setup, the ignition probability is mainly controlled by the loading characteristics subjected to the explosive sample. As stated in the literature Refs.[3,40], the loading characteristics can be extracted from the pressure–time curves (Figs. 7, 8, 9) and are represented by the peak pressure (p), rise time to that pressure (t), and maximum rate of rise (dp/dt).

Moreover, based on the pressure–time curves (as shown in Figs. 7–9), the experimental results can be classified into three categories: NO-GO, GO, and post-peak ignition (PPI). For the NO-GO and PPI scenarios, the parameter p represents the peak pressure on the pressure–time curves, t denotes the rise time to the peak pressure, and dp/dt is calculated as the quotient of p and t. In the GO scenario, p and t correspond to the values at the ignition onset on the pressure–time curves, with dp/dt similarly calculated as the quotient of p and t.

The three loading characteristics (p, t, and dp/dt) can be adjusted by both hammer loading module and pulse shaping module (Fig. 1). According to the impact tests performed on the DNAN-based melt-cast explosive, these loading characteristics are listed in Tables 3 and 4. Notably, the loading characteristics for the explosive samples with confinements A (Table 3) and B (Table 4) are listed separately, as the radial deformation of the explosive sample with confinement A is different from that with confinement B.

The logistic regression analyses were conducted using the scikit-learn library in Python[41].

Evaluation of ignition discrimination

Combining the datasets listed in Tables 3 and 4 with Eq. (1), the logistic regression model was calibrated separately for the datasets of the explosive samples with confinements A and B. The dataset with confinement A consisted of 32 NO-GO and 8 GO/PPI, while the dataset with confinement B consisted of 10 NO-GO and 13 GO/PPI. The calibrated logistic regression model for the datasets with confinements A and B are expressed by

$$P(Y=1|X,\text{Confinement A}) = \frac{1}{1+e^{-(-35.153-0.135p+0.533\frac{dp}{dt})}}, \tag{3}$$

$$P(Y=1|X,\text{Confinement B}) = \frac{1}{1+e^{-(-2.850-0.021p+0.032\frac{dp}{dt})}}. \tag{4}$$

Based on Eqs. (3) and (4), the ignition probability of the DNAN-based melt-cast explosive upon impact can be obtained, given the values of both p and dp/dt.

Figure 12 shows the sensitivity and specificity versus all possible cutoffs for the dataset with confinements A and B using stratified five-fold CV. To choose an optimal cutoff for classification, a simple and commonly used method is to choose a cutoff that maximizes both sensitivity and specificity[35]. This is calculated as the probability cutoff with the maximum value of the Youden's index, defined as (sensitivity + specificity - 1)[42]. A higher value of the Youden's index, a higher discriminative ability of the probability cutoff[38]. As shown in Fig. 12, the optimal choice for the cutoffs ranged from 0.46 to 0.93 and from 0.41 to 0.87 for the datasets with confinements A and B, respectively.

Furthermore, at low cutoffs, the model will yield a large number of true positives (high sensitivity) with a small number of true negatives (low specificity), as shown in Fig. 12. In addition, based on the definitions of both

	Predicted NO-GO	Predicted GO
Actual NO-GO	TN	FP
Actual GO	FN	TP

Table 2. Confusion matrix[39].

No.	Soft confinements (outer diameter: 30 mm, inner diameter: 15 mm)				No.	Soft confinements (outer diameter: 30 mm, inner diameter: 15 mm)			
	p (MPa)	t (ms)	dp/dt (MPa/ms)	Reaction		p (MPa)	t (ms)	dp/dt (MPa/ms)	Reaction
1	636	4.1	156	NO-GO	21	454	5.1	89	NO-GO
2	399	5.1	79	NO-GO	22	470	2.6	177	NO-GO
3	574	4.1	139	NO-GO	23	495	3.9	126	NO-GO
4	504	4.0	127	NO-GO	24	543	4.0	134	NO-GO
5	426	4.5	94	NO-GO	25	415	3.5	118	NO-GO
6	403	4.0	101	NO-GO	26	340	4.0	85	NO-GO
7	589	2.9	202	NO-GO	27	615	3.3	188	NO-GO
8	457	4.6	99	NO-GO	28	439	5.2	85	NO-GO
9	453	4.0	114	NO-GO	29	518	2.9	180	NO-GO
10	613	2.9	209	NO-GO	30	625	2.9	216	NO-GO
11	508	3.4	149	NO-GO	31	553	3.7	150	NO-GO
12	492	3.5	142	NO-GO	32	422	3.4	123	NO-GO
13	564	3.5	163	NO-GO	33	622	2.7	234	GO
14	550	3.4	161	NO-GO	34	771	1.3	607	GO
15	577	3.4	168	NO-GO	35	680	1.8	378	GO
16	564	3.5	162	NO-GO	36	555	2.6	215	GO
17	605	3.1	195	NO-GO	37	266	1.8	146	GO
18	542	3.1	172	NO-GO	38	481	2.3	209	GO
19	484	3.0	164	NO-GO	39	537	2.6	209	PPI
20	518	4.0	131	NO-GO	40	668	1.8	365	PPI

Table 3. Results of the impact test with different pulse shapers under confinement A.

No.	Soft confinements (outer diameter: 20 mm, inner diameter: 15 mm)				No.	Soft confinements (outer diameter: 20 mm, inner diameter: 15 mm)			
	p (MPa)	t (ms)	dp/dt (MPa/ms)	Reaction		p (MPa)	t (ms)	dp/dt (MPa/ms)	Reaction
1	353	2.8	126	NO-GO	13	192	0.5	352	GO
2	395	3.3	121	NO-GO	14	181	0.4	411	GO
3	439	3.2	138	NO-GO	15	309	0.6	480	GO
4	430	2.6	162	NO-GO	16	255	0.6	456	GO
5	442	3.2	139	NO-GO	17	278	0.6	482	GO
6	448	2.8	160	NO-GO	18	202	0.3	732	GO
7	499	5.6	90	NO-GO	19	293	0.6	498	GO
8	347	5.8	59	NO-GO	20	366	1.3	279	GO
9	410	2.8	144	NO-GO	21	224	0.5	481	GO
10	437	2.9	149	NO-GO	22	327	2.9	113	PPI
11	210	0.5	383	GO	23	475	3.2	147	PPI
12	307	1.7	180	GO					

Table 4. Results of the impact test with different pulse shapers under confinement B.

sensitivity and specificity (Section "Load characteristics subjected to the explosive samples"), the sum of TPR and false negative rate is equal to 1. The sum of TNR and false positive rate is also equal to 1. Therefore, at low cutoffs, the model will yield a small number of false negatives with a large number of false positives. In this study, we focused on the ignition discrimination of the explosive samples upon impact. False positive implies that the explosive sample's response NO-GO was incorrectly predicted as GO when the sample suffered from a potential hazard. Similarly, false negative implies that the explosive sample's response GO was incorrectly predicted as NO-GO when the sample suffered from an actual hazard. Therefore, we prefer low cutoffs to minimize the risk of incorrectly predicting GO as NO-GO.

With the help of the above analysis of the cutoff choice, as a rule of thumb, a cutoff of 0.5 was used in this study, and then the mean accuracy of the model was calculated to be 1.0 and 0.92 for ignition discrimination of the explosive samples with confinements A and B, respectively.

Moreover, with the cutoff of 0.5, Fig. 13 shows the corresponding ROC curves and AUC values. For the explosive samples with confinement A, the five ROC curves and their mean value yield an AUC of 0.99 and standard deviation of 0.0, as shown in Fig. 13a. Similarly, for the explosive samples with confinement B, the five ROC curves and their mean value yield an AUC of 0.90 and standard deviation of 0.13, as shown in Fig. 13b.

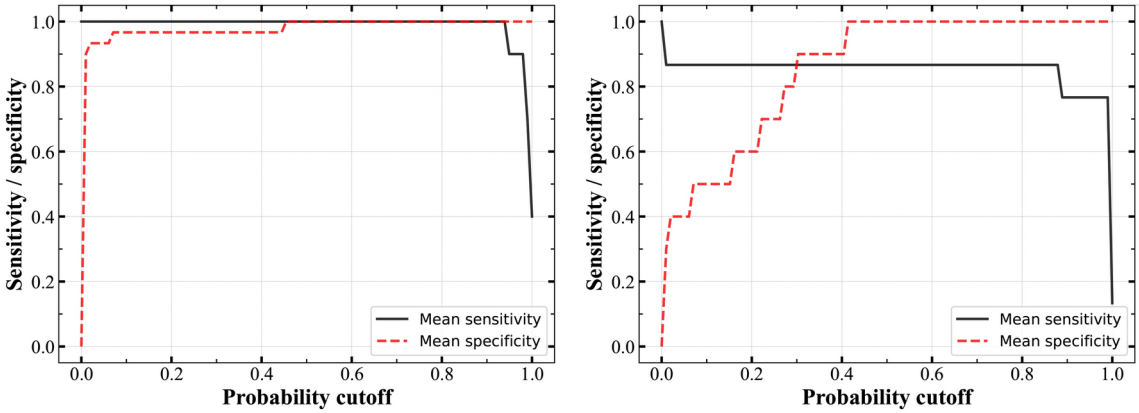

(a) Confinements A **(b)** Confinements B

Fig. 12. Sensitivity and specificity versus all possible cutoffs for confinements A and B using stratified five-fold CV.

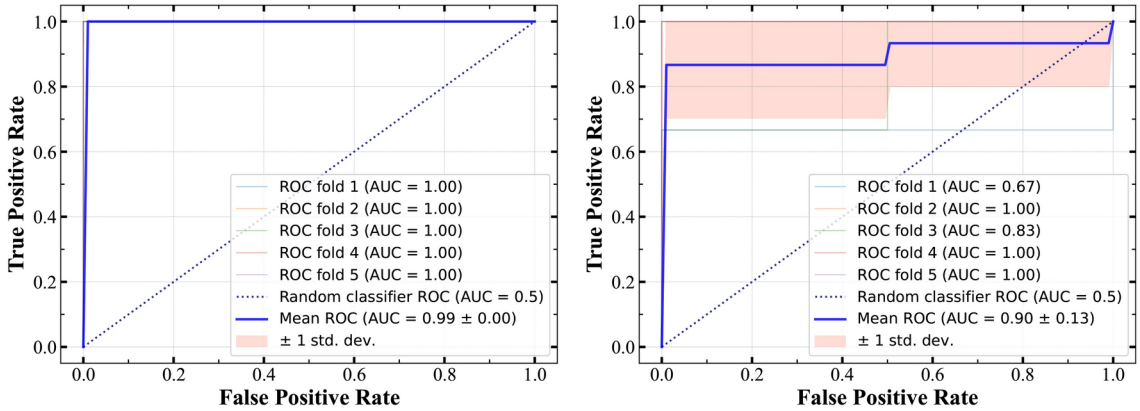

(a) Confinements A **(b)** Confinements B

Fig. 13. ROC curves for stratified five-fold CV.

Compared to the case with confinement A, the standard deviation for the case with confinement B is considerably larger. This difference may be caused by the smaller number of data for the case with confinement B. Additionally, the ROC curve of a random classifier is often included to serve as a comparison point (random classifier ROC). Generally, the rule of thumb is used to measure how well the model can discriminate. AUC values of 0.7 to 0.8 indicate an acceptable discrimination, values of 0.8 to 0.9 indicate an excellent discrimination, and values of $\geq$ 0.9 indicate an outstanding discrimination[35,43]. Therefore, for the explosive samples with confinement either A or B, the model was able to classify the datasets into GO and NO-GO with a very high accuracy.

Conclusion

An impact testing laboratory equipment was developed to assess the safety of a DNAN-based melt-cast explosive upon impact during launch or penetration environment. This equipment is characterized by adjustable loading amplitude ranging from 0.1 to 1.0 GPa and pulse duration ranging from 1 to 8 ms. Compared to other similar equipments[10,13,15,16,44], our equipment can control both loading amplitude and pulse duration more conveniently and efficiently. In addition, this equipment can provide both soft and rigid radial confinements for the explosive samples upon an axial impact.

When the explosive samples were impacted by the drop hammer of the equipment, such mechanical stimulus was measured by a pressure transducer installed at the bottom of the lower plunger, and the corresponding pressure–time history could be obtained. This pressure–time curve can be mainly characterized by the peak pressure (p) and maximum rate of pressure rise (dp/dt).

The response of the explosive samples upon impact depends not only on the loading characteristics (peak pressure (p) and maximum rate of pressure rise (dp/dt)) but also on the radial confinement of the explosive samples. Moreover, the response of the explosive samples can be affected by many random factors, such as the

microstructural morphology of the explosive sample. Therefore, a probabilistic model, i.e., logistic regression model was used to classify the ignition and non-ignition events for the explosive samples upon impact.

The logistic regression model was calibrated separately for DNAN-based melt-cast explosives with confinements A and B. Due to the two datasets exhibited a significant imbalance, a stratified five-fold CV method was used to evaluate this model. For classification performance, a cutoff of 0.5 was used to minimize the risk of incorrectly predicting GO as NO-GO.

Finally, three metrics (accuracy, ROC curve, and AUC) were used to evaluate the classification performance of this model. For the explosive samples with confinement A, the accuracy of this model was 1.0 and the AUC value was 0.99, while, for the explosive samples with confinement B, the accuracy of this model was 0.92 and the AUC value was 0.9. This performance demonstrates that logistic regression effectively evaluates the safety of explosive samples under non-shock mechanical stimuli with varying amplitude and duration.

In future investigations, by combining drop hammer tests using our equipment with the logistic regression model, we can compare the safety of different explosives with known loading characteristics (peak pressure (p) and maximum rate of pressure rise (dp/dt)) subjected to the explosive samples. The safety of one explosive maybe better than that of another explosive at some loading characteristics, but it maybe quite worse at other loading characteristics.

Data availability

The datasets used and/or analysed during the current study available from the corresponding author on reasonable request.

Received: 12 September 2024; Accepted: 25 November 2024
Published online: 30 November 2024

References

1. Cook, M. D. *et al.* An investigation into the mechanisms responsible for delayed detonations in projectile impact experiments. In *Proceedings of the 13th Symposium (International) on Detonation*, 351–07 (2006).
2. Saglam Ozkasapoglu, G. & Onel, S. Investigation of system parameters towards safer impact based shock-to-detonation transition in a novel laser driven flyer plate prototype. *Defence Technol.*[SPACE]https://doi.org/10.1016/j.dt.2024.04.003 (2024).
3. Myers, T. F. The effect of base gaps on setback-shock sensitivities of cast composition B and TNT as determined by the NSWC setback-shock simulator. In *The 7th International Detonation Symposium*, 914–923 (1981).
4. Lecume, S. et al. Survival of high explosives during penetration. *ASME-PUBLICATIONS-PVP* **394**, 161–166 (1999).
5. Jensen, R. C., Blommer, E. J. & Brown, B. An instrumented shotgun facility to study impact initiated explosive reactions. In *The 7th International Detonation Symposium*, 299–307 (Annapolis, 1981).
6. Green, L. G. *et al.* Delayed detonation in propellants from low velocity impact. In *The 7th International Detonation Symposium*, 256–264 (1981).
7. Keefe, R. L. & Works, B. Delayed detonation in card gap tests. In *The 7th International Detonation Symposium*, 265–272 (1981).
8. Ma, X. et al. Measuring crack growth and rise in temperature around a cylindrical defect in explosive simulants under low-pressure and long-pulse loadings. *Propellants Explos. Pyrotech.* **45**, 1654–1661. https://doi.org/10.1002/prep.202000057 (2020).
9. Zhou, L. et al. Test Method for Anti-overload Performance of Explosives. *Acta Armamentarii* **44**, 1722–1732 (2023).
10. Baker, E. Laboratory setback activators and explosive suitability for gun launch. *Probl. Mechatron. Armament Aviat. Saf. Eng.* **10**, 9–24. https://doi.org/10.12783/ballistics2017/16937 (2019).
11. Starkenberg, J., Ervin, L. H. & McFadden, D. L. Air Compression Heating Ignition of High Explosives in the Launch Environment. Technical Report BRL-TR-2709, US Army Ballistic Research Laboratory (1986).
12. Holmes, M. D., Parker, G. R., Dickson, P., Heatwole, E. & Broilo, B. Low-velocity impact ignition of thin metal-cased charges of PBX 9501. *In AIP Conference Proceedings***1979**, 150019. https://doi.org/10.1063/1.5044975 (2018) (**AIP Publishing, St. Louis, MO, USA**).
13. Taylor, B. C., Starkenberg, J. & Ervin, L. H. An experimental investigation of Composition-B ignition under artillery setback conditions. Technical Report ARBRL-TR-02276, US Army Armament Research and Development Command US Army Ballistic Research Laboratory (1980).
14. Sadik, S. Final Report on a Study of Premature Explosions in Artillery Projectiles Filled with Composition-B. Manuscript UCRL-53150, Lawrence Livermore National Lab., United States (1983).
15. Sandusky, H. W. & Granholm, R. H. Violent reactions from non-shock stimuli. *AIP Conf. Proc.* **955**, 991–996. https://doi.org/10.1063/1.2833298 (2007).
16. Liu, W., Wang, G., Rui, X., Li, C. & Wang, Y. A test method for launch safety of explosive charge accurately simulating launch overload. *J. Energ. Mater.*[SPACE]https://doi.org/10.1080/07370652.2022.2108165 (2022).
17. Dai, X. et al. The development of a confined impact test for evaluating the safety of polymer-bonded explosives during warhead penetration. *Propellants Explos. Pyrotech.* **40**, 665–673. https://doi.org/10.1002/prep.201400256 (2015).
18. Zhu, D., Zhou, L., Xiangrong, Z. & Xing, R. Comparison of comprehensive properties for DNAN and TNT-based melt-cast explosives. *Chin. J. Energ. Mater.* **27**, 923–930 (2019).
19. Meng, J.-J., Lin, Z. & Miao, F.-C. Review of the essential characteristics of 2,4-dinitroanisole. *Central Eur. J. Energ. Mater.* **20**, 50–74. https://doi.org/10.22211/cejem/162865 (2023).
20. Cao, T., Zhou, L., Zhang, X., Zhang, W. & Miao, F. Shock initiation characteristics of an aluminized DNAN/RDX melt-cast explosive. *J. Energ. Mater.* **128**, 1–13. https://doi.org/10.1080/07370652.2016.1267277 (2017).
21. Miao, F., Li, D., Cheng, Y., Meng, J. & Zhou, L. Shock initiation experiments with modeling on a DNAN based melt-cast insensitive explosive. *Defence Technol.* **32**, 655–662. https://doi.org/10.1016/j.dt.2023.02.009 (2024).
22. Das, A. Logistic regression. In Maggino, F. (ed.) *Encyclopedia of Quality of Life and Well-Being Research*, 3985–3986, https://doi.org/10.1007/978-3-031-17299-1_1689 (Springer International Publishing, Cham, 2023).
23. Patel, M., Patel, S. & Ahmad, S. Blast analysis of efficient honeycomb sandwich structures with CFRP/steel FML skins. *Int. J. Impact Eng.* **178**, 104609. https://doi.org/10.1016/j.ijimpeng.2023.104609 (2023).
24. Patel, M. & Patel, S. Blast mitigation analysis of novel designed sandwich structures using novel approaches. *Mech. Adv. Mater. Struct.* **31**, 7195–7217. https://doi.org/10.1080/15376494.2023.2243614 (2024).
25. Patel, M. & Patel, S. Assessment of dynamic response of armor grade steel plates and FMLs under air-blast loads. *Mech. Adv. Mater. Struct.*[SPACE]https://doi.org/10.1080/15376494.2024.2382368 (2024).
26. Boyle, M., Pilarski, D. L. & Blake, H. Combined pressure-shear ignition sensitivity test. Tech. Rep. BRL-TR-2927, USA Ballistic Research Laboratory, Aberdeen Proving Ground, MD (1988).

27. Barua, A., Kim, S., Horie, Y. & Zhou, M. Prediction of probabilistic ignition behavior of polymer-bonded explosives from microstructural stochasticity. *J. Appl. Phys.* **113**, 184907. https://doi.org/10.1063/1.4804251 (2013).
28. Van Griensven, F. et al. Evidence of an explosive epidemic of HIV infection in a cohort of men who have sex with men in Thailand. *AIDS* **27**, 825–832. https://doi.org/10.1097/QAD.0b013e32835c546e (2013).
29. Tushar *et al.* A logistic regression and decision tree based hybrid approach to predict alzheimer's disease. In *2023 International Conference on Computational Intelligence and Sustainable Engineering Solutions (CISES)*, 722–726, https://doi.org/10.1109/CISES58720.2023.10183466 (2023).
30. Rifai, A., Prihatni, R. & Sumiati, A. Analysis of financial and non-financial factors on fixed assets revaluation in banking companies. *Interconnect. Econ. Perspect. Horiz.* **1**, 87–99 (2023).
31. Dumitrescu, E., Hué, S., Hurlin, C. & Tokpavi, S. Machine learning for credit scoring: Improving logistic regression with non-linear decision-tree effects. *Eur. J. Oper. Res.* **297**, 1178–1192. https://doi.org/10.1016/j.ejor.2021.06.053 (2022).
32. Niu, L. A review of the application of logistic regression in educational research: Common issues, implications, and suggestions. *Educ. Rev.* **72**, 41–67. https://doi.org/10.1080/00131911.2018.1483892 (2020).
33. Lombardo, L. & Mai, P. M. Presenting logistic regression-based landslide susceptibility results. *Eng. Geol.* **244**, 14–24. https://doi.org/10.1016/j.enggeo.2018.07.019 (2018).
34. Dong, J.-J., Tung, Y.-H., Chen, C.-C., Liao, J.-J. & Pan, Y.-W. Logistic regression model for predicting the failure probability of a landslide dam. *Eng. Geol.* **117**, 52–61 (2011).
35. Hosmer, D. W., Lemeshow, S. & Sturdivant, R. X. *Applied logistic regression*. Wiley Series in Probability and Statistics (John Wiley & Sons, Inc., Hoboken, New Jersey, 2013), third edition edn.
36. Beguería, S. Validation and evaluation of predictive models in hazard assessment and risk management. *Nat. Hazards* **37**, 315–329. https://doi.org/10.1007/s11069-005-5182-6 (2006).
37. Prusty, S., Patnaik, S. & Dash, S. K. SKCV: Stratified K-fold cross-validation on ML classifiers for predicting cervical cancer. *Front. Nanotechnol.* **4**, 972421. https://doi.org/10.3389/fnano.2022.972421 (2022).
38. Aggarwal, R. & Ranganathan, P. Understanding diagnostic tests - part 3: Receiver operating characteristic curves. *Perspect. Clin. Res.* **9**, 145–148. https://doi.org/10.4103/picr.PICR_87_18 (2018).
39. Wardhani, N. W. S., Rochayani, M. Y., Iriany, A., Sulistyono, A. D. & Lestantyo, P. Cross-validation metrics for evaluating classification performance on imbalanced data. In *2019 International Conference on Computer, Control, Informatics and Its Applications (IC3INA)*, 14–18, https://doi.org/10.1109/IC3INA48034.2019.8949568 (2019).
40. Huang, Z., Zhang, J., Zhang, H., Lin, J. & Wu, F. A new criterion for the launching safety of explosive charge. *Acta Armamentarii* **3**, 13–17 (1994).
41. Pedregosa, F. et al. Scikit-learn: Machine learning in python. *J. Mach. Learn. Res.* **12**, 2825–2830 (2011).
42. Fluss, R., Faraggi, D. & Reiser, B. Estimation of the youden index and its associated cutoff point. *Biom. J.* **47**, 458–472. https://doi.org/10.1002/bimj.200410135 (2005).
43. LaValley, M. P. Logistic regression. *Circulation* **117**, 2395–2399. https://doi.org/10.1161/CIRCULATIONAHA.106.682658 (2008).
44. Fishburn, B. Design Modification and Calibration of the Picatinny Activator for Setback Safety Testing of Sadarm. Technical Report ARAED-TR-92001, Energetics and Warheads Division (SMCAR -AEE-WW), Picatinny Arsenal (1992).

Acknowledgements

I sincerely thank Assistant Professor Jun Yu from the School of Mathematics and Statistics at Beijing Institute of Technology for his invaluable guidance on the logistic regression section. His insightful feedback and expertise were instrumental in developing this work. This research was funded by the opening project of the State Key Laboratory of Explosion Science and Safety Protection(Beijing Institute of Technology) grant number YBKT23-08 and KFJJ24-16M.

Author contributions

Conceptualization, Xiangrong Zhang and Lin Zhou; methodology, Wujiang Ying; validation, Zhuoheng Li; investigation, Pan Liu; writing—original draft preparation, Wujiang Ying; writing—review and editing, Xiangrong Zhang; funding acquisition, Feichao Miao and Xiangrong Zhang. All authors have read and agreed to the published version of the manuscript. All authors reviewed the manuscript.

Declarations

Competing interests

The author(s) declare no competing interests.

Additional information

Correspondence and requests for materials should be addressed to X.Z.